# Synchronization in networks with heterogeneous coupling delays

Andreas Otto, Günter Radons, Dániel Bachrathy, and Gábor Orosz

# Synchronization in networks with heterogeneous coupling delays

Andreas Otto[*] and Günter Radons[†]

*Institute of Physics, Chemnitz University of Technology, 09107 Chemnitz, Germany*

Dániel Bachrathy[‡]

*Department of Applied Mechanics, Budapest University of Technology and Economics, H-1111, Budapest, Hungary*

Gábor Orosz[§]

*Department of Mechanical Engineering, University of Michigan, Ann Arbor, MI 48109, USA*

(Dated: January 4, 2018)

Synchronization in networks of identical oscillators with heterogeneous coupling delays is studied. A decomposition of the network dynamics is obtained by block diagonalizing a newly introduced adjacency lag operator which contains the topology of the network as well as the corresponding coupling delays. This generalizes the master stability function approach, which was developed for homogenous delays. As a result the network dynamics can be analyzed by delay differential equations with distributed delay, where different delay distributions emerge for different network modes. Frequency domain methods are used for the stability analysis of synchronized equilibria and synchronized periodic orbits. As an example, the synchronization behavior in a system of delay-coupled Hodgkin-Huxley neurons is investigated. It is shown that the parameter regions where synchronized periodic spiking is unstable expand when increasing the delay heterogeneity.

## I. INTRODUCTION

Complex networks and synchronization phenomena are relevant in many fields. Specific examples can be found in social systems [1, 2], engineering [3–6], biology [7–10] and physics [11–13]. Some universal results on synchronization in complex networks have been summarized in [14, 15]. Often the interactions between nodes in the network are assumed to be instantaneous, which means that the state of one node immediately affects the state of other nodes. However, if the signal propagation time is at the order of the internal time scales of the system, then time delays must be incorporated when modeling the connections between the network nodes. Some basic results on the dynamics of networks with time delayed couplings can be found in [16–18]. In some applications, like semiconductor lasers [11–13], the coupling delays can be tuned to be homogeneous. However, in general, the coupling delays are heterogeneous, i.e., there exist different delays for different connections in the network [5]. Such heterogeneity may affect the stability of synchronized equilibria and synchronized periodic orbits and lead to "amplitude death" in complex networks [19, 20].

Numerical simulations or statistical methods are often used to study the synchronization behavior in networks with heterogeneous delays [20–22]. However, a better understanding of the dynamics can be gained by analyzing the linear stability of specific solutions (equilibria, periodic orbits, heteroclinic orbits, chaotic motion). In particular, decomposing the dynamics into network modes

in the vicinity of a particular solution allows systematic investigations of stability and bifurcations. The so-called master stability function approach combines such modal decomposition with linear stability analysis. This was first proposed for the analysis of completely synchronized solutions in networks with instantaneous couplings [23, 24] where stability properties were linked to the eigenvalues of the adjacency matrix. Similar decompositions were performed for nonidentical node dynamics [25, 26] and around cluster states [27–29].

Modal decomposition can be extended to networks with delay couplings [17]. This is possible even for multiple delays [30–32], and distributed delays in the connections [33]. However, in all these cases the delays were considered to be homogeneous, that is, the same delay distribution was used for all connections. An extension to heterogeneous delays was given in [34] with the restriction that the adjacency matrices corresponding to different coupling delays must commute. Another approach based on a timescale separation was presented for hierarchical networks having a small coupling delay within subnetworks and a large coupling delay between subnetworks [35]. A general approach for the modal decomposition around synchronized equilibria with heterogeneous coupling delays was introduced in [5]. Extending this method to synchronized time dependent solutions is not straightforward and we target this challenging problem in this paper.

We introduce the so-called adjacency lag operator that describes the topology of the network as well as the corresponding coupling delays. By block diagonalizing this operator we decompose the network dynamics and show that the network modes are given by non-autonomous delay differential equations (DDEs) with distributed delay in the vicinity of completely synchronized time dependent solutions. The advantage of the proposed method

[*] otto.a@mail.de

[†] radons@physik.tu-chemnitz.de

[‡] bachrathy@mm.bme.hu

[§] orosz@umich.edu

is that, similar to the classical master stability approach used for networks with homogeneous delay, the number of DDEs describing the dynamics of a network mode is equal to the number of equations describing a network node. We show that for heterogeneous delay coupling the delay distributions arising in the modal DDEs may be different for each mode. This is in contrast to the classical master stability approach, where the modal equations only differ in a complex number (eigenvalue of the adjacency matrix).

In the context of complex networks, synchronous periodic oscillations of neurons are of special importance [7–10, 14]. Some results for synchronized solutions of networks of Hodgkin-Huxley neurons with homogeneous coupling delays were presented in [8, 10]. Here we apply the developed decomposition method to study the effects of heterogeneous coupling delays on such neural dynamics. For the stability analysis of synchronized periodic solutions we use a frequency domain approach that has been successfully applied in other applications like machine tool vibrations [36, 37].

The paper is organized as follows. In Sec. II conditions for the existence of synchronized solutions in heterogeneous delay-coupled networks are given. In Sec. III the decomposition of the dynamics around time dependent solutions is performed. This is combined with numerical continuation in Sec. IV in order to study the stability and bifurcations of synchronized periodic orbits in a network of Hodgkin-Huxley neurons. We conclude our results in Sec. V.

## II. SYNCHRONIZATION IN NETWORKS WITH HETEROGENEOUS DELAYS

A network of $N$ identical oscillators with heterogeneous delay coupling is considered. In particular, $R$ different coupling delays are considered. Indeed, $R = 1$ gives the special case of homogeneous delays. The state of the nodes are described by $\boldsymbol{x}_i \in \mathbb{R}^n$, $i = 1 \ldots N$ while the coupling delays are denoted by $\tau_r$, $r = 1, \ldots, R$. The dynamics of node $i$ is modeled by the nonlinear DDE

$$\dot{\boldsymbol{x}}_i(t) = \boldsymbol{f}\big(\boldsymbol{x}_i(t)\big) + \sum_{r=1}^{R}\sum_{j=1}^{N} a_{r,ij}\, \boldsymbol{g}\big(\boldsymbol{x}_i(t), \boldsymbol{x}_j(t - \tau_r)\big). \quad (1)$$

The dynamics of the uncoupled node is described by the $n$ dimensional nonlinear ordinary differential equation (ODE) $\dot{\boldsymbol{x}}_i = \boldsymbol{f}(\boldsymbol{x}_i)$, while the coupling function $\boldsymbol{g}(\boldsymbol{x}_i, \boldsymbol{x}_j)$ specifies how oscillator $j$ influences the dynamics of oscillator $i$. The coefficients $a_{r,ij}$ are the elements of the $N$-dimensional coupling matrices $\mathbf{A}_r$ corresponding to the delay $\tau_r$. They specify how strong the current state $\boldsymbol{x}_i(t)$ of node $i$ is affected by the delayed state $\boldsymbol{x}_j(t - \tau_r)$ of node $j$ with time delay $\tau_r$. According to the modeling framework, if $a_{r,ij} = 0$ then there is no signal going from node $j$ to node $i$ with time delay $\tau_r$, but a signal may travel between the same nodes with another delay. Note

that to incorporate continuous distributions for the coupling delays the first sum in Eq. (1) is replaced by an integral. Still, often we have $a_{r,ij} \neq 0$ for a single $r$ only. The sum $\sum_{r=1}^{R} \mathbf{A}_r = \mathbf{A}$ is the delay-independent coupling matrix. It characterizes the network via a weighted directed graph, where the oscillators are represented as nodes and the coupling between them are represented as edges. The weights of the edges are specified by the entries in the matrix $\mathbf{A}$, but there is no information on the coupling delays in $\mathbf{A}$.

### A. Synchronization

In this paper completely synchronized solutions of Eq. (1) are studied which are contained in the so-called synchronization manifold defined by $\boldsymbol{x}_i(t) = \boldsymbol{x}_s(t)$, $i = 1, \ldots, N$. The dynamics within this manifold is described by the DDE

$$\dot{\boldsymbol{x}}_s(t) = \boldsymbol{f}\big(\boldsymbol{x}_s(t)\big) + \sum_{r=1}^{R} M_r\, \boldsymbol{g}\big(\boldsymbol{x}_s(t), \boldsymbol{x}_s(t - \tau_r)\big), \quad (2)$$

where $M_r$ denotes the constant row sum of the coupling matrix $\mathbf{A}_r$, i.e.,

$$M_r := \sum_{j=1}^{N} a_{r,ij}, \quad \text{for } i = 1, \ldots, N. \quad (3)$$

If for some coupling matrix $\mathbf{A}_r$ the row sum is not independent of the row index $i$, then it is not possible to define the synchronization manifold.

In the special case of homogeneous delays ($R = 1$), Eq. (2) simplifies to

$$\dot{\boldsymbol{x}}_s(t) = \boldsymbol{f}\big(\boldsymbol{x}_s(t)\big) + M_1\, \boldsymbol{g}\big(\boldsymbol{x}_s(t), \boldsymbol{x}_s(t - \tau_1)\big). \quad (4)$$

In this case, the condition Eq. (3) means that the row sum $M$ of the delay-independent coupling matrix $\mathbf{A}$ has to be independent of the row index $i$. In general, $M$ is defined by

$$M := \sum_{r=1}^{R}\sum_{j=1}^{N} a_{r,ij}, \quad \text{for } i = 1, \ldots, N. \quad (5)$$

As a consequence, time dependent synchronized states may exist for homogeneous delays (when Eq. (5) holds) but may be destroyed when adding heterogeneity to the delays (when Eq. (3) is not satisfied). Moreover, for the existence of synchronized time-independent solutions (equilibria) having Eq. (5) is already sufficient as will be discussed below.

To analyze the stability of synchronized solutions we define the perturbations $\boldsymbol{y}_i(t) = \boldsymbol{x}_i(t) - \boldsymbol{x}_s(t)$ whose dynamics can be approximated by the linear variational system

$$\dot{\boldsymbol{y}}_i(t) = \mathbf{L}(t)\, \boldsymbol{y}_i(t) + \sum_{r=1}^{R}\sum_{j=1}^{N} a_{r,ij}\, \mathbf{R}(t, \tau_r)\, \boldsymbol{y}_j(t - \tau_r), \quad (6)$$

in the vicinity of the synchronized solution. The coefficient matrices are defined as

$$\mathbf{L}(t) = \mathrm{D}\boldsymbol{f}\big(\boldsymbol{x}_{\mathrm{s}}(t)\big) + \sum_{r=1}^{R} M_r \, \mathrm{D}_1 \boldsymbol{g}\big(\boldsymbol{x}_{\mathrm{s}}(t), \boldsymbol{x}_{\mathrm{s}}(t - \tau_r)\big),$$
$$\mathbf{R}(t, \tau) = \mathrm{D}_2 \boldsymbol{g}\big(\boldsymbol{x}_{\mathrm{s}}(t), \boldsymbol{x}_{\mathrm{s}}(t - \tau)\big),$$
$$(7)$$

where $\mathrm{D}\boldsymbol{f}$ is the Jacobian of $\boldsymbol{f}$, and the matrices $\mathrm{D}_1\boldsymbol{g}$ and $\mathrm{D}_2\boldsymbol{g}$ are the derivatives of $\boldsymbol{g}$ with respect to the first and the second argument, respectively. Defining the $nN$ dimensional column vector $\boldsymbol{y} = \mathrm{col}\,[\boldsymbol{y}_1, \ldots, \boldsymbol{y}_N]$, Eq. (6) can be rewritten as

$$\dot{\boldsymbol{y}}(t) = \big(\mathbf{I}_N \otimes \mathbf{L}(t)\big)\boldsymbol{y}(t) + \sum_{r=1}^{R} \big(\mathbf{A}_r \otimes \mathbf{R}(t, \tau_r)\big)\boldsymbol{y}(t - \tau_r), \quad (8)$$

where $\otimes$ denotes the Kronecker product and $\mathbf{I}_N$ denotes the $N$-dimensional identity matrix.

At this point, one may notice an important consequence of heterogeneous delays. In this case, despite the same coupling function $\boldsymbol{g}$ appearing in all connections and for all delays in Eq. (1), the coefficient matrices $\mathbf{R}(t, \tau_r)$ in the linearized dynamics Eq. (6) depend on the coupling delays $\tau_r$ through $\boldsymbol{x}_{\mathrm{s}}(t - \tau_r)$. This has consequences for the decomposability of the network dynamics, as will discussed in Sec. III.

### B. Tangential vs. transversal dynamics

The perturbation vector $\boldsymbol{y}$ in Eq. (8) can be divided into tangential perturbations and transversal perturbations [23, 24, 28]. For tangential perturbations, each node undergoes the same perturbation $\boldsymbol{y}_i(t) = \boldsymbol{q}_1(t)$ for $i = 1, \ldots, N$, that is, $\boldsymbol{y}(t) = \mathrm{col}[\boldsymbol{q}_1(t), \ldots, \boldsymbol{q}_1(t)]$. Substituting this into (6) one obtains the dynamics for perturbations within the synchronization manifold

$$\dot{\boldsymbol{q}}_1(t) = \mathbf{L}(t)\boldsymbol{q}_1(t) + \sum_{r=1}^{R} M_r \, \mathbf{R}(t, \tau_r) \, \boldsymbol{q}_1(t - \tau_r), \quad (9)$$

that is indeed the linearization of Eq. (2). The transversal perturbations are defined as $\boldsymbol{y}_i(t) \neq \boldsymbol{y}_j(t)$ for at least one $i \neq j$.

Indeed, many different solutions may exist within the infinite dimensional synchronization manifold (equilibria, periodic orbits, homoclinic and heteroclinic orbits, chaos). Whereas tangential perturbations let the system stay within the synchronization manifold, transversal perturbations drive the system away from the synchronization manifold. Synchronization occurs only if the synchronized solution is transversally stable. The linearized dynamics of the network and its decomposition are discussed in detail in Sec. III.

### C. Synchronized equilibria without synchronization manifold

Time delays can change the stability of an equilibrium but do not change the existence and location of the equilibrium [38, 39]. According to Eq. (1) synchronized equilibria $\boldsymbol{x}_{\mathrm{s}}(t) \equiv \boldsymbol{x}_{\mathrm{s}}^*$ of the network are given by

$$\boldsymbol{f}\big(\boldsymbol{x}_{\mathrm{s}}^*\big) + M \, \boldsymbol{g}\big(\boldsymbol{x}_{\mathrm{s}}^*, \boldsymbol{x}_{\mathrm{s}}^*\big) = 0, \quad (10)$$

where $M$ is defined by Eq. (5). Thus, as long as Eq. (5) holds, changing the delays of the connections does not change the existence of synchronized equilibria. On the other hand, according to Eq. (3) changing the delays can change the existence of time dependent synchronized solutions. In other words, synchronized equilibria exist if the constant row sum condition is fulfilled for the delay-independent coupling matrix $\mathbf{A}$ but time dependent synchronized solution exist only if the constant row sum condition is fulfilled for all coupling matrices $\mathbf{A}_r$, $r = 1, \ldots, R$. We remark that if the coupling is non-invasive at the synchronized solution, i.e. $\boldsymbol{g}\big(\boldsymbol{x}_{\mathrm{s}}^*, \boldsymbol{x}_{\mathrm{s}}^*\big) = 0$, synchronized equilibria may also exist independent of the specific network topology and independent of the coupling delays.

As a consequence, there is a large set of networks with heterogeneous delays, where synchronized equilibria exist but no time dependent synchronized solutions are possible. In these cases, no synchronization manifold can be defined and no tangential network mode exists. Indeed, if all transversal perturbations around the equilibrium decay then the synchronized equilibrium is stable but when the equilibrium becomes unstable, an asynchronous state appears. In these networks stable synchronized equilibria occur due of identical node dynamics and identical or non-invasive coupling functions which is often referred to as amplitude death in the literature [40–42]. An overview on the different scenarios including the possibility for synchronized equilibria without a synchronization manifold is presented in Fig. 1. Finally, recall that Eq. (5) also ensures the existence of time dependent synchronized solutions for homogeneous delays but Eq. (3) is needed to ensure this for heterogeneous delays. That is by making delays heterogenous one may destroy the synchronization manifold while still keeping the synchronized equilibria.

### III. DECOMPOSITION OF NETWORKS WITH HETEROGENEOUS COUPLING DELAYS

Characterizing the stability of completely synchronized solutions requires the analysis Eq. (8). However, for large networks investigating Eq. (8) directly is typically not feasible. To solve this problem, and to gain insight into the network dynamics, we will decompose the dynamics into a tangential mode (see Eq. (9)) and $N-1$ transversal modes. For networks with homogeneous delay $(R = 1)$, the decomposition can be carried out with the help of the diagonalization of the adjacency matrix $\mathbf{A} = \mathbf{A}_1$ [17,
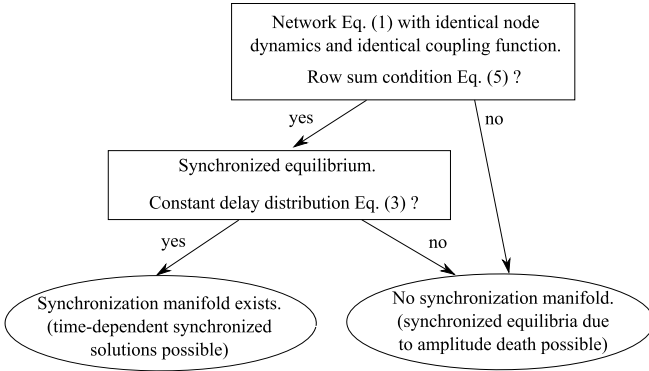
FIG. 1. Complete synchronization and amplitude death in networks with heterogeneous delays.

23, 24, 28]. For networks with heterogeneous delays the same decomposition is still possible if all matrices $\mathbf{A}_r$, $r = 1, \ldots, R$ commute with each other [34]. However, in most cases the matrices $\mathbf{A}_r$ do not commute.

A general approach for decomposition was introduced in [5] for the analysis of synchronized equilibria based on the eigenmode decomposition of the matrix

$$\hat{\mathbf{B}}(s) = \sum_{r=1}^{R} \mathbf{A}_r \, \mathrm{e}^{-s\tau_r}, \tag{11}$$

which can be derived from the Laplace domain representation of Eq. (8) ($s \in \mathbb{C}$ is the Laplace variable) and combines the information on the coupling topology and the coupling delays. However, we will show below that for time-dependent synchronized solutions such decomposition is not possible in general. Thus, in this paper we carry out the decomposition in the time domain using lag operators and emphasize the fundamental limitations caused by the time dependency of the matrices $\mathbf{L}(t)$ and $\mathbf{R}(t, \tau)$.

### A. Three decomposition levels

Delay-coupled networks are infinite dimensional systems due to the existence of time delays $\tau_r$ in the coupling terms, i.e., the initial condition for Eq. (8) is a function on the time interval $[-\tau_{\max}, 0]$ for the vector $\boldsymbol{y} \in \mathbb{R}^{nN}$, where $\tau_{\max}$ is the maximum delay. This means that the state at time $t$ can be defined by the function $\boldsymbol{y}(t + \theta)$, $-\tau_{\max} \leq \theta \leq 0$ [43, 44]. Roughly speaking the network is $N \times n \times \infty$ dimensional.

According to this, three different levels of decomposition of delay-coupled networks may be identified. The first level is the network level, which focuses on the $N$ nodes coupled via the edges of the graph. A decomposition at the network level decomposes the dynamics into $N$ network modes. If Eq. (3) is fulfilled, one tangential and $N-1$ transversal network modes exist [10, 17, 23, 24].

The second level is the node level corresponding to the $n$ dimensional system specifying the dynamics at each node, which may be decomposed into $n$ decoupled scalar DDEs; see [45, 46] where the scalar Lambert W function was utilized. For example, one may decompose Eq. (9) for the tangential dynamics into $n$ scalar DDEs. A decomposition combining the network and the node level is possible but in such a case the corresponding modes are less descriptive. The third level is the delay level. In particular, a scalar DDE can be further decomposed into infinitely many ODEs corresponding to the characteristic roots [43, 47, 48]. The node level and the delay level are often handled together using Operator Differential Equations [43] or Matrix Lambert W function [49].

In the remaining part of this paper we focus on the decomposition at the network level. Indeed, such a decomposition is not always possible. For example, networks with non-identical node dynamics, i.e., using $\boldsymbol{f}_i$ instead of $\boldsymbol{f}$ in Eq. (1) yield $\mathbf{L}_i$ instead of $\mathbf{L}$ in Eq. (6). In this case, the Kronecker product in Eq. (8) cannot be constructed and a decomposition at the network level is not possible in general.

### B. Representation with lag operators

We are searching for a time domain representation of the network dynamics in terms of an operator that contains the information about the network topology as well as the coupling delays similar to the matrix $\hat{\mathbf{B}}(s)$ defined in Eq. (11).

Let us introduce the lag operator $\mathcal{S}(\tau)$ defined by

$$\mathcal{S}(\tau) \, y(t) = y(t - \tau), \tag{12}$$

for a scalar-valued function $y(t)$. Indeed, this can be extended to vector valued functions. An alternative representation of the lag operator can be derived from the Taylor expansion of $y(t - \tau)$ about $\tau = 0$ and is given by $\mathcal{S}(\tau) = \mathrm{e}^{-\tau \frac{d}{dt}}$. The eigenfunctions of the lag operator are exponential functions independent of the time lag, that is,

$$\mathcal{S}(\tau) \, \mathrm{e}^{st} = \mathrm{e}^{-s\tau} \, \mathrm{e}^{st}, \tag{13}$$

where $s \in \mathbb{C}$. As a consequence, lag operators with different arguments commute with each other and fulfill the relation

$$\mathcal{S}(\tau_1) \mathcal{S}(\tau_2) = \mathcal{S}(\tau_2) \mathcal{S}(\tau_1) = \mathcal{S}(\tau_1 + \tau_2). \tag{14}$$

It follows that $\mathcal{S}^n(\tau) = \mathcal{S}(n\tau)$ and the identity element is denoted by $\mathcal{S}(0)$. Obviously, the lag operator commutes with the differential operator $\frac{d}{dt}\mathcal{S}(\tau) = \mathcal{S}(\tau)\frac{d}{dt}$.

With the help of the lag operator, the linearized dynamics Eq. (8) can be written as

$$\dot{\boldsymbol{y}}(t) = \left( \mathbf{I}_N \otimes \mathbf{L}(t) + \sum_{r=1}^{R} \mathbf{A}_r \, \mathcal{S}(\tau_r) \otimes \mathbf{R}(t, \tau_r) \right) \boldsymbol{y}(t). \tag{15}$$

We remark that when calculating the elements of the Kronecker product $\mathbf{A}_r \mathcal{S}(\tau_r) \otimes \mathbf{R}(t, \tau_r)$ the lag operators do not act on $\mathbf{R}(t, \tau_r)$; see (8). Since the matrix $\mathbf{R}(t, \tau_r)$ may be different for each term in the sum in Eq. (15), decomposition at the network level is not possible in general. In this paper we focus on the case when the coefficient matrix $\mathbf{R}(t, \tau) = \mathbf{R}(t)$ does not depend on the delay $\tau$. This occurs, for example, in the case of synchronized equilibria $\boldsymbol{x}_s(t) = \boldsymbol{x}_s(t - \tau) \equiv \boldsymbol{x}_s^*$, which results in constant matrix $\mathbf{R} = \mathbf{D}_2 \boldsymbol{g}(\boldsymbol{x}_s^*, \boldsymbol{x}_s^*)$. Also, when the coupling is in the form $\boldsymbol{g}(\boldsymbol{x}_i(t), \boldsymbol{x}_j(t - \tau_r)) = \mathbf{G}(\boldsymbol{x}_i(t)) \cdot \boldsymbol{x}_j(t - \tau_r)$, we obtain $\mathbf{R}(t) = \mathbf{G}(\boldsymbol{x}_s(t))$. In these cases Eq. (15) can be simplified to

$$\dot{\boldsymbol{y}}(t) = (\mathbf{I}_N \otimes \mathbf{L}(t) + \mathcal{B} \otimes \mathbf{R}(t)) \boldsymbol{y}(t), \qquad (16)$$

where the so-called adjacency lag operator $\mathcal{B}$ is defined by

$$\mathcal{B} = \sum_{r=1}^{R} \mathbf{A}_r \, \mathcal{S}(\tau_r). \qquad (17)$$

This contains all information about the network topology (given by the matrices $\mathbf{A}_r$) and the coupling delays (specified by the lag operators $\mathcal{S}(\tau_r)$). Notice that the matrix $\hat{\mathbf{B}}(s)$ defined in Eq. (11) is the Laplace domain representation of the adjacency lag operator $\mathcal{B}$.

## C. Decomposition of the adjacency lag operator

The adjacency lag operator $\mathcal{B}$ contains lag operators defined in Eq. (12). Due to the property (14) these operators can be handled like commuting symbols. First we present the formal diagonalization of the operator $\mathcal{B}$ that is equivalent to the diagonalization of the matrix $\hat{\mathbf{B}}(s)$ presented in [5]. We also show that this does not necessarily decouple the linearized dynamics around time dependent synchronized solutions and we present an alternative approach for the decomposition to overcome this problem.

Let us search for a diagonalization of the adjacency lag operator $\mathcal{B}$ as

$$\begin{aligned} \mathcal{B}\,\mathcal{V}_k &= \mathcal{D}_k\,\mathcal{V}_k, \\ \mathcal{U}_k\,\mathcal{B} &= \mathcal{D}_k\,\mathcal{U}_k, \quad k = 1, \ldots, N, \end{aligned} \qquad (18)$$

where $\mathcal{D}_k$ is a scalar operator serving as the "eigenvalue" while $\mathcal{V}_\ell$ and $\mathcal{U}_k$ are vector valued operators in column and row format (with $N$ components) serving as the "right and left eigenvectors". These form an orthonormal system with $\mathcal{U}_k \cdot \mathcal{V}_\ell = \delta_{k\ell}$, where $\cdot$ represents the $N$-dimensional dot product and $\delta_{k\ell}$ denotes the Kronecker delta. In general, $\mathcal{D}_k$, $\mathcal{V}_k$, $\mathcal{U}_k$ may contain linear and nonlinear functions of the lag operators $\mathcal{S}(\tau_r)$. We assume that the diagonalization Eq. (18) exists, i.e., algebraic and geometric multiplicities are the same for each eigenvalue $\mathcal{D}_k$.

Using eigenvectors $\mathcal{V}_k$ and $\mathcal{U}_k$ we define the new variables

$$\boldsymbol{q}_k(t) = (\mathcal{U}_k \otimes \mathbf{I}_n)\,\boldsymbol{y}(t), \qquad (19)$$

and use them to construct the solution of Eq. (16) as

$$\boldsymbol{y}(t) = \sum_{\ell=1}^{N} (\mathcal{V}_\ell \otimes \mathbf{I}_n)\,\boldsymbol{q}_\ell(t). \qquad (20)$$

Then, by multiplying Eq. (16) with $\mathcal{U}_k \otimes \mathbf{I}_n$ from the left, substituting Eq. (20), and using Eqs. (18) (19) yields

$$\dot{\boldsymbol{q}}_k(t) = \sum_{\ell=1}^{N} (\mathcal{U}_k\,[\mathbf{L}(t)]\,\mathcal{V}_\ell + \mathcal{U}_k\,[\mathbf{R}(t)]\,\mathcal{V}_\ell \mathcal{D}_\ell) \boldsymbol{q}_\ell(t), \quad (21)$$

where we used the abbreviated notation $\mathcal{U}_k\,[\mathbf{P}(t)]\,\mathcal{V}_\ell = (\mathcal{U}_k \otimes \mathbf{P}(t))(\mathcal{V}_\ell \otimes \mathbf{I}_n)$ where only the lag operators in $\mathcal{U}_k$ act on $\mathbf{P}(t)$.

If the coefficient matrices $\mathbf{L}(t) = \mathbf{L}_0$ and $\mathbf{R}(t) = \mathbf{R}_0$ are time independent (which happens around synchronized equilibria [5]), then $\mathcal{U}_k\,[\mathbf{L}_0]\,\mathcal{V}_\ell = \mathbf{L}_0\,\delta_{k\ell}$ and $\mathcal{U}_k\,[\mathbf{R}_0]\,\mathcal{V}_\ell = \mathbf{R}_0\,\delta_{k\ell}$. As a consequence, Eq. (21) decouples into $N$ independent subsystems, where $\boldsymbol{q}_k$ and $\mathcal{V}_k$ act as modal coordinates and mode shapes, respectively. In contrast, for time dependent coefficient matrices $\mathcal{U}_k\,[\mathbf{L}(t)]\,\mathcal{V}_\ell \neq \mathbf{L}(t)\,\delta_{k\ell}$ and $\mathcal{U}_k\,[\mathbf{R}(t)]\,\mathcal{V}_\ell \neq \mathbf{R}(t)\,\delta_{k\ell}$ since $\mathcal{U}_k$ and $\mathcal{V}_k$ can contain lag operators. (A paradigmatic example for such a coupling term can be given by $\mathcal{U}_k\,[\mathbf{L}(t)]\,\mathcal{V}_\ell = \mathbf{L}(t) - \mathbf{L}(t - \tau_r)$ for $k \neq l$.) Thus, even if the adjacency lag operator $\mathcal{B}$ can be diagonalized, the network dynamics Eq. (16) does not automatically decouple into $N$ subsystems when writing it in terms of the modal coordinates Eq. (21).

Nevertheless, it is worth taking a closer view at Eq. (21). Often $\mathcal{V}_k$ and/or $\mathcal{U}_k$ does not contain lag operators (but numbers only). This happens if the coupling matrices $\mathbf{A}_r$, $r = 1, \ldots, R$ have common eigenvectors (either right or left). In such cases, the corresponding operator is given by

$$\mathcal{D}_k = \sum_{r=1}^{R} \sigma_{r,k}\,\mathcal{S}(\tau_r), \qquad (22)$$

where $\sigma_{r,k}$, $r = 1, \ldots, R$ are the eigenvalues of the matrices $\mathbf{A}_r$, $r = 1, \ldots, R$ belonging to the common eigenvector of the $k$th network mode. As a consequence, many of the coupling terms in Eq. (21) vanish as illustrated in Fig. 2(a). In particular, we distinguish between three different types of modes.

We first consider the modes $k = 1, \ldots, k_1$, where the left eigenvectors $\mathcal{U}_k$ contain only numbers. Then we have $\mathcal{U}_k\,[\mathbf{L}(t)]\,\mathcal{V}_\ell = \mathbf{L}(t)\,\delta_{k\ell}$ and $\mathcal{U}_k\,[\mathbf{R}(t)]\,\mathcal{V}_\ell = \mathbf{R}(t)\,\delta_{k\ell}$ and Eq. (21) simplifies to

$$\dot{\boldsymbol{q}}_k(t) = (\mathbf{L}(t) + \mathbf{R}(t)\,\mathcal{D}_k) \boldsymbol{q}_k(t). \qquad (23)$$

for $k = 1, \ldots, k_1$. In other words, the first $k_1$ modes are completely decoupled; see the top rows in Fig. 2(a).
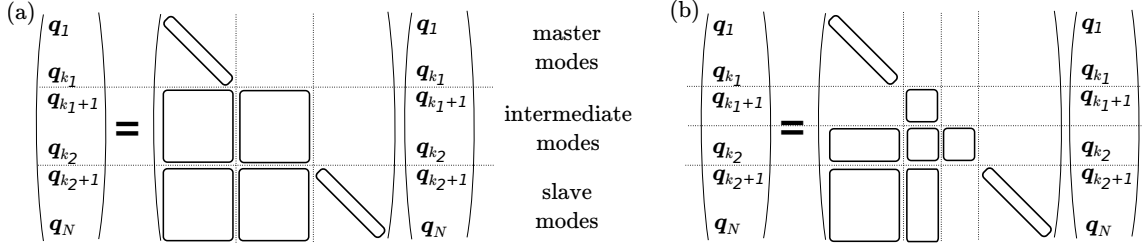
FIG. 2. (a) Structure of Eq. (21) with separation into master modes ($\mathcal{U}_k$ contains only numbers), slave modes ($\mathcal{V}_k$ contains only numbers) and intermediate modes. Only the squares and the diagonal stripes are non-empty. The stripes at the main diagonal are associated with Eq. (23) and determine the stability of the master and the slave modes, respectively. The intermediate modes are driven by the master modes and both can drive the slave modes. (b) Structure of Eq. (21) after additional decomposition of the intermediate modes. The two small squares at the main diagonal of the intermediate modes are associated with two blocks similar to Eq. (25), specifying the stability of the intermediate modes.

We call these *master modes* because they can drive the remaining modes of the network. Note that Eq. (22) yields $\mathcal{D}_k\, \boldsymbol{q}_k(t) = \sum_{r=1}^{R} \sigma_{r,k}\, \boldsymbol{q}_k(t - \tau_r)$. Thus, Eq. (23) is a DDE with distributed delay with kernel $\sum_{r=1}^{R} \sigma_{k,r}\, \delta(\tau - \tau_r)$, where $\delta$ denotes the Dirac delta function.

Second, we consider the modes $k = k_2 + 1, \ldots, N$, where the right eigenvectors $\mathcal{V}_k$ contain only numbers while the left eigenvectors $\mathcal{U}_k$ contain lag operators. In this case, we have $\mathcal{U}_k\,[\mathbf{L}(t)]\,\mathcal{V}_\ell = \mathbf{L}(t)\,\delta_{k\ell}$ and $\mathcal{U}_k\,[\mathbf{R}(t)]\,\mathcal{V}_\ell = \mathbf{R}(t)\,\delta_{k\ell}$ for $\ell = k_2 + 1, \ldots, N$ and the corresponding coupling terms vanish in Eq. (21); see the last columns in Fig. 2(a). As these modes do not drive any other mode but can be driven by other modes we call them *slave modes*. Note that if the driving modes are zero, Eq. (23) would describe the slave modes. We remark that the tangential mode is always a slave mode because $\mathcal{V}_1 = [\, 1, \ldots, 1\, ]^{\mathrm{T}}$ meaning that the tangential mode cannot drive transversal modes.

The third type of modes with $k = k_1 + 1, \ldots, k_2$ are called *intermediate modes* shown in the middle rows in Fig. 2(a). In this case both $\mathcal{U}_k$ and $\mathcal{V}_k$ contain lag operators and the dynamics of the intermediate modes is not decoupled as illustrated by the large block in the middle in Fig. 2(a). In order to decouple the intermediate modes from each other, a modified decomposition of the adjacency lag operator $\mathcal{B}$ different from the eigenmode decomposition Eq. (18) is necessary.

More precisely, we aim for the block diagonalization of the adjacency lag operator $\mathcal{B}$ such that for the intermediate modes $k = p, \ldots, q$ we have

$$
\begin{aligned}
\mathcal{B}\, \mathcal{V}_{p,\ldots,q} &= \mathcal{D}_{p,\ldots,q}\, \mathcal{V}_{p,\ldots,q}, \\
\mathcal{U}_{p,\ldots,q}\, \mathcal{B} &= \mathcal{D}_{p,\ldots,q}\, \mathcal{U}_{p,\ldots,q}.
\end{aligned}
\tag{24}
$$

Here $\mathcal{D}_{p,\ldots,q}$ is a $Q \times Q$ block of lag operators ($Q = q - p + 1 > 1$), $\mathcal{V}_{p,\ldots,q}$ and $\mathcal{U}_{p,\ldots,q}$ represent operator blocks of size $N \times Q$ and $Q \times N$, respectively, and $\mathcal{U}_{p,\ldots,q} \cdot \mathcal{V}_{p,\ldots,q}$ gives the $Q$ dimensional identity matrix. Specifically, we construct Eq. (24) such that either $\mathcal{U}_{p,\ldots,q}$ or $\mathcal{V}_{p,\ldots,q}$ contain only numbers. Then, due to common invariant right or left subspaces of the coupling matrices $\mathbf{A}_r$, $r = 1, \ldots, R$, the

elements of $\mathcal{D}_{p,\ldots,q}$ are given by linear combinations of the lag operators $\mathcal{S}(\tau_r)$.

As a consequence, the intermediate modes can be further decomposed into intermediate master modes (when $\mathcal{U}_{p,\ldots,q}$ contains only numbers) and intermediate slave modes (when $\mathcal{V}_{p,\ldots,q}$ contains only numbers); see Fig. 2(b). Then, the dynamics of the intermediate master modes is given by

$$
\dot{\boldsymbol{q}}_{p,\ldots,q}(t) = \big(\mathbf{I}_Q \otimes \mathbf{L}(t) + \mathcal{D}_{p,\ldots,q} \otimes \mathbf{R}(t)\big)\boldsymbol{q}_{p,\ldots,q}(t), \tag{25}
$$

where $\boldsymbol{q}_{p,\ldots,q}(t)$ has $n\,Q$ components. Note that such equation also describes the intermediate slave modes if the driving modes were zero.

We conclude that, in contrast to the case of synchronized equilibria, for time dependent synchronized solutions the diagonalization of the adjacency lag operator $\mathcal{B}$ given by Eq. (18) does not automatically decouple the network modes. Instead, a block triangular structure arises as shown in Fig. 2. Using the block diagonalization given by Eq. (24) further decomposition of the intermediate modes may be possible. Then the stability of the synchronized solution can be guaranteed by ensuring that the blocks on the main diagonal decay exponentially, i.e., the solutions of Eq. (23) for the master and slave modes and also the solutions of Eq. (25) for the intermediate modes decay exponentially. A frequency domain method for stability analysis of these systems is presented in Appendix A.

### D. Examples

As an illustration, two examples with $N = 5$ nodes and two different coupling delays are presented. The first one is a special case of all-to-all coupling without self-coupling. In particular, we consider the coupling matrices

$$\mathbf{A}_1 = \begin{bmatrix} 0 & 1 & 1 & 1 & 0 \\ 1 & 0 & 0 & 1 & 1 \\ 1 & 0 & 0 & 1 & 1 \\ 1 & 1 & 1 & 0 & 0 \\ 0 & 1 & 1 & 1 & 0 \end{bmatrix}, \quad \mathbf{A}_2 = \begin{bmatrix} 0 & 0 & 0 & 0 & 1 \\ 0 & 0 & 1 & 0 & 0 \\ 0 & 1 & 0 & 0 & 0 \\ 0 & 0 & 0 & 0 & 1 \\ 1 & 0 & 0 & 0 & 0 \end{bmatrix}, \quad (26)$$

that result in the adjacency matrix

$$\mathbf{A} = \mathbf{A}_1 + \mathbf{A}_2 = \begin{bmatrix} 0 & 1 & 1 & 1 & 1 \\ 1 & 0 & 1 & 1 & 1 \\ 1 & 1 & 0 & 1 & 1 \\ 1 & 1 & 1 & 0 & 1 \\ 1 & 1 & 1 & 1 & 0 \end{bmatrix}, \quad (27)$$

and the adjacency lag operator

$$\mathcal{B} = \mathbf{A}_1 \mathcal{S}(\tau_1) + \mathbf{A}_2 \mathcal{S}(\tau_2)$$
$$= \begin{bmatrix} 0 & \mathcal{S}(\tau_1) & \mathcal{S}(\tau_1) & \mathcal{S}(\tau_1) & \mathcal{S}(\tau_2) \\ \mathcal{S}(\tau_1) & 0 & \mathcal{S}(\tau_2) & \mathcal{S}(\tau_1) & \mathcal{S}(\tau_1) \\ \mathcal{S}(\tau_1) & \mathcal{S}(\tau_2) & 0 & \mathcal{S}(\tau_1) & \mathcal{S}(\tau_1) \\ \mathcal{S}(\tau_1) & \mathcal{S}(\tau_1) & \mathcal{S}(\tau_1) & 0 & \mathcal{S}(\tau_2) \\ \mathcal{S}(\tau_2) & \mathcal{S}(\tau_1) & \mathcal{S}(\tau_1) & \mathcal{S}(\tau_1) & 0 \end{bmatrix}, \quad (28)$$

cf. (17). Notice that for this example the adjacency matrix $\mathbf{A}$ is symmetric but the adjacency lag operator $\mathcal{B}$ is not as $\mathcal{B}_{45} \neq \mathcal{B}_{54}$.

After diagonalization of $\mathcal{B}$ described by Eq. (18) the operator-valued eigenvalues are

$$\begin{aligned} \mathcal{D}_1 &= 3\mathcal{S}(\tau_1) + \mathcal{S}(\tau_2), \\ \mathcal{D}_2 &= -2\mathcal{S}(\tau_1) + \mathcal{S}(\tau_2), \\ \mathcal{D}_3 &= -\mathcal{S}(\tau_1), \\ \mathcal{D}_4 &= -\mathcal{S}(\tau_2), \\ \mathcal{D}_5 &= -\mathcal{S}(\tau_2). \end{aligned} \quad (29)$$

Each $\mathcal{D}_k$ is a linear combination of the lag operators $\mathcal{S}(\tau_1)$ and $\mathcal{S}(\tau_2)$ so that their coefficients are indeed the eigenvalues of $\mathbf{A}_1$ and $\mathbf{A}_2$ ( belonging to a common eigenvector); cf. Eq. (22). The corresponding operators $\mathcal{U}_k$ and $\mathcal{V}_k$ can be found in Appendix B. Observe that for each $k$, $\mathcal{U}_k$ and/or $\mathcal{V}_k$ contains only numbers and consequently we only have four master modes (2,3,4,5) and one slave mode (1). One may also notice the algebraic multiplicity $\mathcal{D}_4 = \mathcal{D}_5$ that also results in geometric multiplicity. This means that $\mathcal{V}_4$ and $\mathcal{V}_5$ (and similarly $\mathcal{U}_4$ and $\mathcal{U}_5$) are not unique but here they are constructed such that orthonormality is satisfied.

The second example is referred to as general coupling and is defined by the coupling matrices

$$\mathbf{A}_1 = \begin{bmatrix} 0 & 1 & 1 & 1 & 0 \\ 1 & 0 & 0 & 1 & 1 \\ 1 & 0 & 0 & 1 & 1 \\ 1 & 1 & 1 & 0 & 0 \\ 0 & 1 & 1 & 1 & 0 \end{bmatrix}, \quad \mathbf{A}_2 = \begin{bmatrix} 0 & 0 & 0 & 0 & 1 \\ 0 & 0 & 1 & 0 & 0 \\ 0 & 1 & 0 & 0 & 0 \\ 0 & 0 & 0 & 0 & 1 \\ 1 & 0 & 0 & 0 & 0 \end{bmatrix}, \quad (30)$$

resulting in the adjacency matrix

$$\mathbf{A} = \mathbf{A}_1 + \mathbf{A}_2 = \begin{bmatrix} 0 & 1 & 0 & 1 & 1 \\ 0 & 0 & 1 & 1 & 1 \\ 1 & 1 & 0 & 0 & 1 \\ 1 & 0 & 1 & 0 & 1 \\ 1 & 1 & 0 & 1 & 0 \end{bmatrix}, \quad (31)$$

and the adjacency lag operator

$$\mathcal{B} = \mathbf{A}_1 \mathcal{S}(\tau_1) + \mathbf{A}_2 \mathcal{S}(\tau_2)$$
$$= \begin{bmatrix} 0 & \mathcal{S}(\tau_1) & 0 & \mathcal{S}(\tau_1) & \mathcal{S}(\tau_2) \\ 0 & 0 & \mathcal{S}(\tau_2) & \mathcal{S}(\tau_1) & \mathcal{S}(\tau_1) \\ \mathcal{S}(\tau_1) & \mathcal{S}(\tau_2) & 0 & 0 & \mathcal{S}(\tau_1) \\ \mathcal{S}(\tau_1) & 0 & \mathcal{S}(\tau_1) & 0 & \mathcal{S}(\tau_2) \\ \mathcal{S}(\tau_2) & \mathcal{S}(\tau_1) & 0 & \mathcal{S}(\tau_1) & 0 \end{bmatrix}. \quad (32)$$

cf. (17).

The diagonalization described in Eq. (18) yields the operator-valued eigenvalues

$$\begin{aligned} \mathcal{D}_1 &= 2\mathcal{S}(\tau_1) + \mathcal{S}(\tau_2), \\ \mathcal{D}_2 &= -\mathcal{S}(\tau_1) + \mathcal{S}(\tau_2), \\ \mathcal{D}_3 &= -\mathcal{S}(\tau_2), \\ \mathcal{D}_4 &= \tfrac{1}{2}\Big( - \big(\mathcal{S}(\tau_1) + \mathcal{S}(\tau_2)\big) \\ &\quad + \sqrt{\mathcal{S}^2(\tau_2) - 2\mathcal{S}(\tau_1)\mathcal{S}(\tau_2) - 3\mathcal{S}^2(\tau_1)}\Big), \\ \mathcal{D}_5 &= \tfrac{1}{2}\Big( - \big(\mathcal{S}(\tau_1) + \mathcal{S}(\tau_2)\big) \\ &\quad - \sqrt{\mathcal{S}^2(\tau_2) - 2\mathcal{S}(\tau_1)\mathcal{S}(\tau_2) - 3\mathcal{S}^2(\tau_1)}\Big), \end{aligned} \quad (33)$$

Here $\mathcal{D}_1$, $\mathcal{D}_2$, and $\mathcal{D}_3$ are linear combination of the lag operators, while $\mathcal{D}_4$ and $\mathcal{D}_5$ are not and can only be defined via multi-variable Taylor series [5]. One can conclude that mode 3 is a master mode, modes 1 and 2 are slave modes and modes 4 and 5 are intermediate modes; see the corresponding operators $\mathcal{U}_k$ and $\mathcal{V}_k$ in Appendix B

As mentioned above the formal diagonalization of $\mathcal{B}$ does not necessarily lead to uncoupled dynamics for the intermediate modes in case of time dependent solutions. Thus, $\mathcal{D}_4$ and $\mathcal{D}_5$ can only be used for the stability analysis of synchronized equilibria. For time dependent synchronized solutions the block diagonalization defined by Eq. (25) is needed, which yields

$$\mathcal{D}_{4,5} = \begin{bmatrix} -\mathcal{S}(\tau_1) & \mathcal{S}(\tau_1) \\ -\mathcal{S}(\tau_1) & -\mathcal{S}(\tau_2) \end{bmatrix}, \quad (34)$$

while the operators $\mathcal{U}_{4,5}$ and $\mathcal{V}_{4,5}$ are given in Appendix B. These are constructed as a linear combination of $\mathcal{U}_4$ and $\mathcal{U}_5$ and as a linear combination of $\mathcal{V}_4$ and $\mathcal{V}_5$. Indeed, the formal diagonalization of $\mathcal{D}_{4,5}$ lead to the operator-valued eigenvalues $\mathcal{D}_4$ and $\mathcal{D}_5$ defined in Eq. (33).

## IV. DELAY-COUPLED HODGKIN-HUXLEY NEURONS

In this section we study the synchronized solutions in a network of $N$ delay-coupled Hodgkin-Huxley neurons with heterogeneous delays [8, 10, 50]. We utilize the modal decomposition from Sec. III and analyze the modal dynamics Eq. (23) and Eq. (25) rather than the full network dynamics Eq. (8). We use the frequency domain method from Appendix A for the stability analysis of the arising non-autonomous DDEs with distributed delay. Apart from having smaller systems for stability analysis the network modes give information about the arising patterns of oscillations when stability is lost.

The time evolution of the Hodgkin-Huxley neuronal network is given by the DDE

$$
\begin{aligned}
C\dot{V}_i(t) = {} & I - g_{\text{Na}}\, m_i^3(t)\, h_i(t)\big(V_i(t) - V_{\text{Na}}\big) \\
& - g_{\text{K}}\, n_i^4(t)\, \big(V_i(t) - V_{\text{K}}\big) \\
& - g_{\text{L}}\, \big(V_i(t) - V_{\text{L}}\big) \\
& + \sum_{r=1}^{R} a_{r,ij}\,\frac{\kappa}{N}\big(V_j(t - \tau_r) - V_i(t)\big), \\
\dot{m}_i = {} & \alpha_m\big(V_i(t)\big)\big(1 - m_i(t)\big) - \beta_m\big(V_i(t)\big)m_i(t), \\
\dot{h}_i = {} & \alpha_h\big(V_i(t)\big)\big(1 - h_i(t)\big) - \beta_h\big(V_i(t)\big)h_i(t), \\
\dot{n}_i = {} & \alpha_n\big(V_i(t)\big)\big(1 - n_i(t)\big) - \beta_n\big(V_i(t)\big)n_i(t),
\end{aligned}
\tag{35}
$$

for $i = 1, \ldots, N$. Here the time $t$ is measured in ms. The symbol $V_i$ denotes the voltage of the $i$-th neuron at the soma (measured in mV) while the dimensionless gating variables $m_i, h_i, n_i \in [0, 1]$ characterize the "openness" of the ion channels embedded in the cell membrane. The specific form of the nonlinear functions $\alpha_m(V)$, $\alpha_h(V)$, $\alpha_n(V)$ and $\beta_m(V)$, $\beta_h(V)$, $\beta_n(V)$ are given in Eq. (C1), while the reference voltages $V_{\text{Na}}$, $V_{\text{K}}$, $V_{\text{L}}$, the conductances $g_{\text{Na}}$, $g_{\text{K}}$, $g_{\text{L}}$, the membrane capacitance $C$, and the driving current $I$ are given in Table I in Appendix C. The last term in the voltage equation in Eq. (35) represents a direct electronic connection of conductance $\kappa$ between the axon of the $j$-th neuron and the dendrites of the $i$-th neuron, that is, $V_i(t)$ represents the postsynaptic potential while $V_j(t - \tau_r)$ represents the presynaptic potential and the delay $\tau_r$ stands for the signal propagation time along the axon of the $j$-th neuron (dendritic delays are omitted here). That is, the presynaptic potential is equal to what the potential of the soma of the $j$th neuron was $\tau_r$ time before.

In order to demonstrate the decomposition techniques established above the examples with all-to-all coupling Eq. (28) and the general coupling Eq. (32) are considered with the conductances fixed at $\kappa = 1.2\frac{\text{mS}}{\text{cm}^2}$ and $\kappa = 1.6\frac{\text{mS}}{\text{cm}^2}$, respectively. The different values of the coupling strengths compensate the different row sums of the two coupling schemes, i.e., $\kappa M$ is the same in the two examples cg. (5). Consequently, the tangential dynamics

Eq. (9) are equivalent in the two cases when considering homogeneous delays $\tau_1 = \tau_2$; see [10]. We vary the delays and study how the stability of the equilibria and periodic soutions change.

### A. Synchronized equilibria

For the parameters considered here, Eq. (35) has a unique equilibrium; see [10]. Fig. 3(a) and (b) show the stability charts for the equilibrium in the $(\tau_1, \tau_2)$-plane for all-to-all coupling (Eq. (28)) and general coupling (Eq. (32)), respectively. The stable domains are shaded. When crossing the thick black curves starting from a shaded domain, the dominant characteristic roots corresponding to the tangential network mode cross the imaginary axis and the synchronized equilibrium bifurcates to synchronized periodic solutions. Notice that along the diagonal $\tau_1 = \tau_2$ of homogeneous delays, tangential stability losses occur at the same locations in both panels. When crossing the thin colored curves, characteristic roots corresponding to transversal network modes cross the imaginary axis. When starting from a shaded domain, the synchronized equilibrium becomes unstable with respect to transversal perturbations and synchronization is broken. In this case typically cluster-synchronized periodic solutions appear [51].

In order to emphasize the effects of delay heterogeneity we show the real part $\lambda$ of the dominant characteristic roots for the case with general coupling in Fig. 4. In Fig. 4(a) and (b) we vary the delays along $\tau_1 = \tau_2$ and along $\tau_2 = \tau_1 + 4.8$ ms shown as dotted and dashed lines in Fig. 3(b), respectively. For the homogeneous case $\tau_1 = \tau_2$ both tangential and transversal stability losses occur and the synchronized equilibrium is stable only for $\tau_1 \in [1.7, 2.4]$ and $\tau_1 \in [3.9, 4.5]$. For the heterogeneous case $\tau_2 = \tau_1 + 4.8$ ms tangential instabilities vanish but transversal ones appear leading to the stable regions $\tau_1 \in [0, 2.4]$ and $\tau_1 \in [7.1, 9.8]$. Note that in this case introducing heterogeneity in the delays increases the stable regions. While this may not be true in general, tuning delay distributions were also used to stabilize the equilibrium for metal cutting [52–54].

### B. Synchronous periodic spiking

Here we study the synchronized periodic solutions embedded within the synchronization manifold. In particular, with the help of the software package DDE-BIFTOOL [55] we compute periodic solutions of Eq. (2) by using numerical collocation and continue these while varying the delays. In Fig. 5 the peak-to-peak voltage amplitude $|V_s|$ of the synchronized periodic solution is plotted as a function of the delay $\tau_1$ for different values of the delay heterogeneity $\Delta\tau = \tau_2 - \tau_1$. The left and the right columns in Fig. 5 correspond to the all-to-all (Eq. (28)) and the general coupling (Eq. (32)), respec-
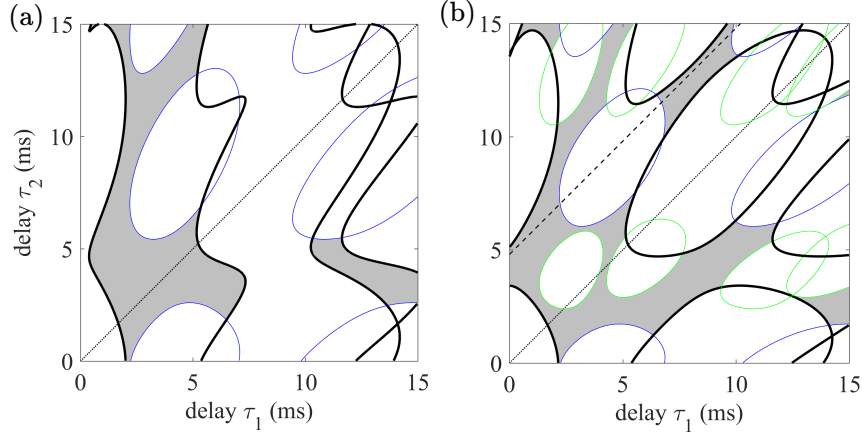
FIG. 3. Stability charts for the equilibrium of Hodgkin-Huxley neurons with (a) all-to-all coupling and (b) general coupling. Thick (black) curves are associated with purely imaginary roots of the tangential mode. Thin dark (blue) and light (green) curves indicate purely imaginary roots associated with mode 2 and 4/5, respectively. Stable regions, where all characteristic roots have negative real part, are shaded. The dotted and dashed lines in panel (b) correspond to Fig. 4(a) and (b), respectively.
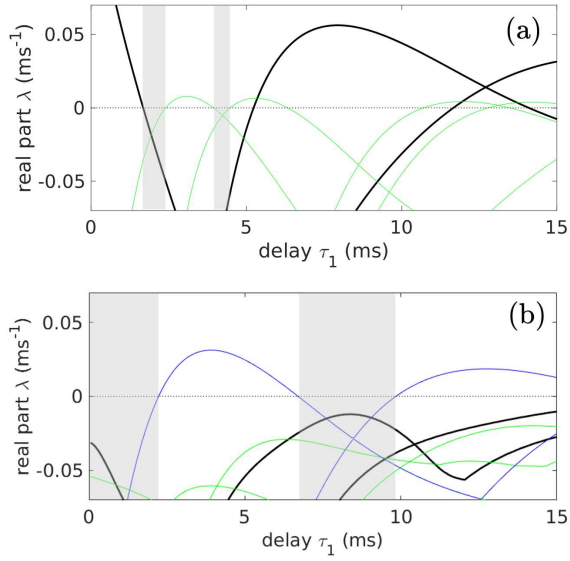


FIG. 4. Real part of characteristic roots for general coupling with (a) homogeneous delays $\tau_1 = \tau_2$ and (b) heterogeneous delays $\tau_2 = \tau_1 + 4.8$ ms (b); cf. Fig. 3(b). Stable regions are shaded. Color code as in Fig. 3 (only the dominant roots corresponding to modes 1,2 and 4/5 are shown).

tively. Notice that the branches are the same in the two columns except the coloring.

DDE-BIFTOOL gives the stability information with respect to the tangential perturbations of the periodic solution: solid thin green (thick red) curves indicate tangentially stable (unstable) solutions. To determine stability with respect to transversal perturbations we decompose the network dynamics as presented in Sec. III and analyze the periodic DDEs with distributed delay given

by Eq. (23) or Eq. (25). The coefficient matrices $\mathbf{L}(t)$ and $\mathbf{R}(t)$ are calculated using the output of DDE-BIFTOOL and the operators $\mathcal{D}_k$ are obtained from (29) for all-to-all coupling and from (33) and (34) for general coupling. Then the dominant Floquet exponents associated with all $N - 1$ transversal network modes are calculated via Hill's infinite determinant Eq. (A10) and the corresponding transversal instabilities are marked by dotted thick black curves in Fig. 5.

The homogeneous delay case $\tau_1 = \tau_2$ is shown in Fig. 5(a) and (b). In this case the red and green coloring is the same in the two panels as the tangential dynamics are equivalent. However, the stability with respect to transversal perturbations (dotted thick black curves) differs due to different eigenvalues of the adjacency lag operator for the two different coupling schemes. For example, at $\tau_1 = \tau_2 = 3.4$ ms (marked by vertical dashed lines) both the synchronized equilibrium ($|V_s| = 0$ mV) and synchronized periodic spiking ($|V_s| \approx 90$ mV) are linearly stable for all-to-all coupling, whereas for general coupling the synchronized equilibrium is unstable.

When increasing the delay heterogeneity $\Delta\tau = \tau_2 - \tau_1$ the parameter regions where the synchronized periodic solutions are unstable expand and in some cases they do not even exist. For example, for $\Delta\tau = 4.8$ ms shown in Fig. 5(i) and (j) no such solutions exist for $\tau_1 \in [1.9, 5.9]$ ms and for $\tau_1 \in [1.4, 6.2]$ ms, respectively. Moreover, transversal instabilities are more pronounced for the case of general coupling. For example, for $\Delta\tau = 4.8$ synchronized periodic spiking is stable for $\tau_1 \in [0, 1.5]$ ms and $\tau_1 \in [6.0, 14.7]$ ms when using all-to-all coupling (see Fig. 5(i)), while for general coupling this motion is only stable for $\tau_1 \in [0, 0.7]$ ms and $\tau_1 \in [6.4, 13.5]$ ms (see Fig. 5(j)).

In order to demonstrate the full nonlinear dynamics of the Hodgkin-Huxley neurons we use numerical sim-
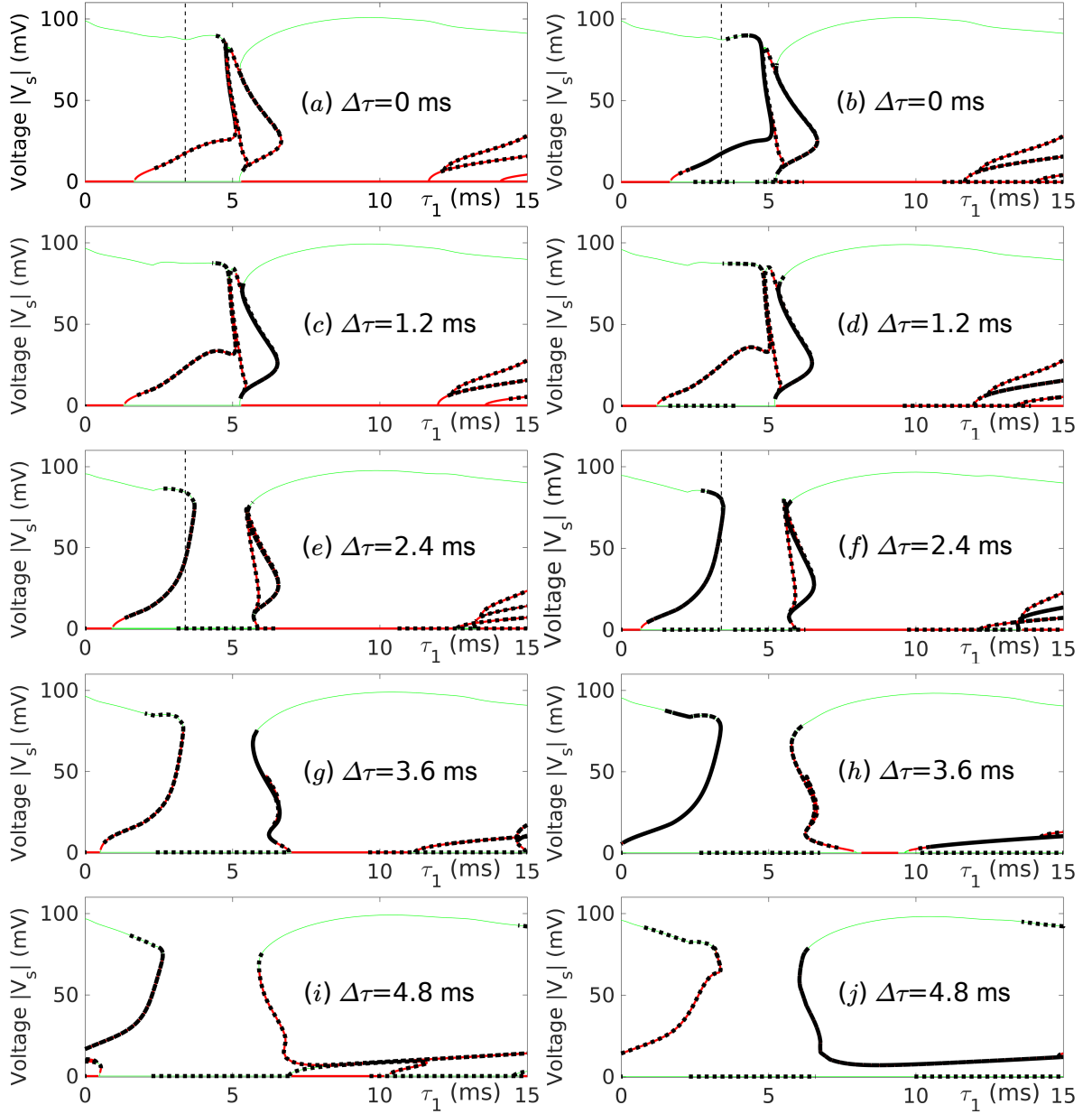
FIG. 5. Bifurcation diagrams for synchronized solutions of the Hodgkin-Huxley neurons for all-to-all coupling (left) and general coupling (right) and different values of the delay heterogeneity $\Delta\tau = \tau_2 - \tau_1$. The peak-to-peak voltage amplitude $|V_s|$ of the synchronized solutions are plotted as a function of the delay $\tau_1$. Solid thin green (thick red) curves represent stable (unstable) solutions with respect to tangential perturbations, while transversal instabilities are marked by dotted black curves. The parameters indicated by the dashed vertical lines in panels (a,b,e,f) are used in Fig. 6.

ulations. Specifically, Eq. (35) is integrated numerically with a Runge-Kutta method [56]. Arbitrary constant values are chosen for the initial functions. For $t < 200$ ms the delays are set to the homogeneous case $\tau_1 = \tau_2 = 3.4$ ms corresponding to the vertical dashed lines in Fig. 5(a) and (b). The voltages $V_i$ of the five neurons are plotted as a function of time $t$ for all-to-all coupling in Fig. 6(a) and for general coupling in Fig. 6(b). In both cases (after some transient dynamics not shown in Fig. 6) syn-

chronized periodic spiking arise. At $t = 200$ ms, the delay $\tau_2$ is increased abruptly to create the heterogeneity $\Delta\tau = \tau_2 - \tau_1 = 2.4$ ms corresponding to the vertical dashed lines in Fig. 5(e) and (f). Since in this case all possible synchronized solutions are transversally unstable, cluster-synchronized periodic spiking appears for the all-to-all coupling and asynchronous spiking appears for the general coupling.
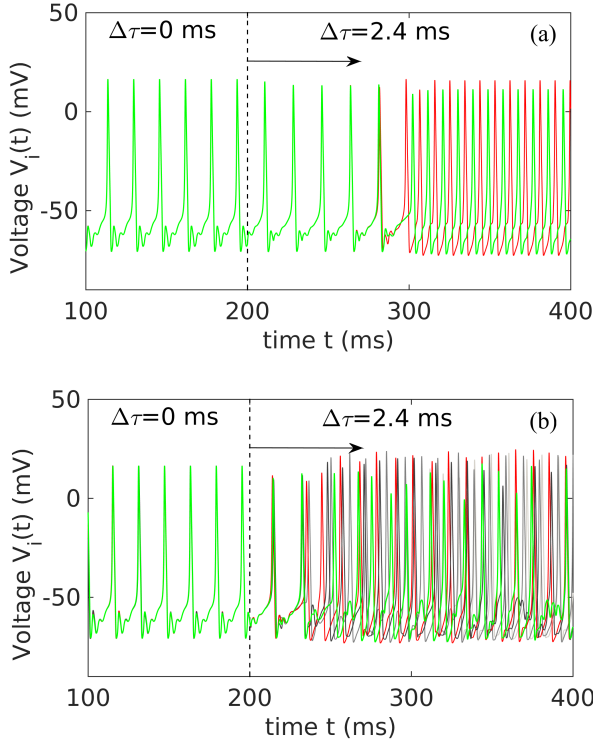
FIG. 6. Voltages of the Hodgkin-Huxley neurons Eq. (35) for all-to-all coupling (a) and general coupling (b). We set $\tau_1 = 3.4$ ms while heterogeneity in the delays is introduced at $t = 200$ ms by switching from $\Delta\tau = 0$ ms to $\Delta\tau = 2.4$ ms.

## V. CONCLUSION

Synchronized solutions of networks with heterogeneous coupling delays were investigated. The conditions for the existence of the synchronization manifold were given. It was shown that adding heterogeneity in the delays may destroy time dependent synchronized solutions while still maintain synchronized equilibria.

A systematic method was presented for the decomposition of the dynamics at the network level in the vicinity of synchronized solutions. This was based on the decomposition of the adjacency lag operator, which contains information about the network topology as well as the coupling delays. In the generic case, the block diagonalization of the adjacency lag operator led to a triangular structure for the modal dynamics. This allowed us to investigate the stability of time dependent synchronized solutions by analyzing the stability of modal DDEs separately, where different modes were associated with different delay distributions.

As an example, the effects of delay heterogeneity on synchronized equilibria and synchronized periodic spiking in a systems of Hodgkin-Huxley neurons were studied. In this case increasing heterogeneity in the coupling delays led to larger regions where all synchronized periodic solutions were unstable or even no synchronized periodic solutions existed. As neurosystems often store information using periodic cluster-synchronized states, establishing mathematical tool for their stability analysis in the presence of heterogeneous delays is an interesting future research direction. The extension of the current work to near synchronous states is another topic left for future research.

[1] X. Li, Y. Y. Jin, and G. Chen, Physica A **328**, 287 (2003).

[2] A. Pluchino, V. Latora, and A. Rapisarda, Int. J. Mod. Phys. C **16**, 515 (2005).

[3] M. Rohden, A. Sorge, M. Timme, and D. Witthaut, Phys. Rev. Lett. **109**, 064101 (2012).

[4] F. M. Atay, Phil. Trans. Royal Soc. A **371** (2013).

[5] R. Szalai and G. Orosz, Phys. Rev. E **88**, 040902 (2013).

[6] K. Schmietendorf, J. Peinke, R. Friedrich, and O. Kamps, Eur. Phys. J. Spec. Top. **223**, 2577–2592 (2014).

[7] L. Glass, Nature **410**, 277 (2001).

[8] E. Rossoni, Y. Chen, M. Ding, and J. Feng, Phys. Rev. E **71**, 061904 (2005).

[9] E. Schöll, G. Hiller, P. Hövel, and M. A. Dahlem, Phil. Trans. Royal Soc. A **367**, 1079 (2009).

[10] G. Orosz, in *Delay Systems*, Advances in Delays and Dynamics, Vol. 1, edited by T. Vyhlídal, J.-F. Lafay, and R. Sipahi (Springer, 2014) pp. 343–357.

[11] S. Zhu, X. Chen, X. Lu, K. S. Thornburg Jr., G. D. Vanwiggeren, and R. Roy, in *Frontiers of Laser Physics and Quantum Optics*, edited by Z. Xu, S. Xie, S.-Y. Zhu, and M. Scully (Springer, 2000) pp. 631–634.

[12] T. Heil, I. Fischer, W. Elsässer, J. Mulet, and C. R. Mirasso, Phys. Rev. Lett. **86**, 795 (2001).

[13] V. Flunkert and E. Schöll, New J. Phys. **14**, 033039 (2012).

[14] A. Pikovsky, M. Rosenblum, and J. Kurths, *Synchronization: A Universal Concept in Nonlinear Sciences* (Cambridge University Press, 2003).

[15] A. Arenas, A. Díaz-Guilera, J. Kurths, Y. Moreno, and C. Zhou, Phys. Rep. **469**, 93 (2008).

[16] F. M. Atay, J. Jost, and A. Wende, Phys. Rev. Lett. **92**, 144101 (2004).

[17] V. Flunkert, S. Yanchuk, T. Dahms, and E. Schöll, Phys. Rev. Lett. **105**, 254101 (2010).

[18] M. Lakshmanan and D. V. Senthilkumar, *Dynamics of Nonlinear Time-Delay Systems* (Springer, 2011).

[19] F. M. Atay, Phys. Rev. Lett. **91**, 094101 (2003).

[20] C. Masoller and A. Mart'ı, Phys. Rev. Lett. **94**, 134102 (2005).

[21] A. Panchuk, D. P. Rosin, P. Hövel, and E. Schöll, Int. J. Bifur. Chaos **23**, 1330039 (2013).

[22] C. Cakan, J. Lehnert, and E. Schöll, Eur. Phys. J. B **87**, 54 (2014).

[23] L. M. Pecora and T. Carroll, Phys. Rev. Lett. **80**, 2109 (1998).

[24] L. M. Pecora, Phys. Rev. E **58**, 347 (1998).

[25] J. Sun, E. M. Bollt, and T. Nishikawa, EPL **85**, 60011 (2009).

[26] F. Sorrentino and M. Porfiri, EPL **93**, 50002 (2011).

[27] T. Dahms, J. Lehnert, and E. Schöll, Phys. Rev. E **86**, 016202 (2012).

[28] G. Orosz, SIAM J. Appl. Dyn. Sys. **13**, 1353 (2014).

[29] L. M. Pecora, F. Sorrentino, A. M. Hagerstrom, T. E. Murphy, and R. Roy, Nat. Commun **5**, 4079 (2014).

[30] A. Englert, W. Kinzel, Y. Aviad, M. Butkovski, I. Reidler, M. Zigzag, I. Kanter, and M. Rosenbluh, Phys. Rev. Lett. **104**, 114102 (2010).

[31] K. Konishi, H. Kokame, and N. Hara, Phys. Rev. E **81**, 016201 (2010).

[32] M. Zigzag, M. Butkovski, A. Englert, W. Kinzel, and I. Kanter, Phys. Rev. E **81**, 036215 (2010).

[33] A. Gjurchinovski, A. Zakharova, and E. Schöll, Phys. Rev. E **89**, 032915 (2014).

[34] A. Englert, S. Heiligenthal, W. Kinzel, and I. Kanter, Phys. Rev. E **83**, 046222 (2011).

[35] O. D'Huys, S. Zeeb, T. Jüngling, S. Heiligenthal, S. Yanchuk, and W. Kinzel, EPL **103**, 10013 (2013).

[36] A. Otto and G. Radons, Proc. 9th Int. Conf. on HSM, San Sebastian, Spain (2012).

[37] D. Bachrathy and G. Stépán, CIRP Annals **62**, 411 (2013).

[38] S. Gurevich and R. Friedrich, Phys. Rev. Lett. **110**, 014101 (2013).

[39] S. Gurevich, Phys. Rev. E **87**, 052922 (2013).

[40] P. C. Matthews and S. H. Strogatz, Phys. Rev. Lett. **65**, 1701 (1990).

[41] D. V. Ramana Reddy, A. Sen, and G. L. Johnston, Phys. Rev. Lett. **85**, 3381 (2000).

[42] V. Resmi, G. Ambika, and R. E. Amritkar, Phys. Rev. E **84**, 046212 (2011).

[43] G. Stépán, *Retarded Dynamical Systems: Stability and Characteristic Functions* (Longman Scientific & Technical, 1989).

[44] J. K. Hale and S. M. Verduyn Lunel, *Introduction to Functional Differential Equations*, Appl. Math. Sci. No. 99 (Springer, 1993).

[45] C. Hwang and Y.-C. Cheng, Automatica **41**, 1979 (2005).

[46] E. Jarlebring and T. Damm, Automatica **43**, 2124 (2007).

[47] R. Bellmann and K. L. Cooke, *Differential-Difference Equations* (Academic Press, 1963).

[48] A. Amann, E. Schöll, and W. Just, Physica A: Stat. Mech. Appl. **373**, 191 (2007).

[49] S. Yi, P. W. Nelson, and A. G. Ulsoy, *Time Delay Systems: Analysis and Control Using the Lambert W Function* (World Scientific, 2010).

[50] A. L. Hodgkin and A. F. Huxley, Journal of Physiology **117**, 500 (1952).

[51] A. Otto, *Frequency domain methods for the analysis of time delay systems*, Ph.D. thesis, TU Chemnitz (2016).

[52] Z. Dombovári, Y. Altintas, and G. Stépán, Int. J. Mach. Tools Manuf. **50**, 511 (2010).

[53] Z. Dombovári and G. Stépán, ASME. J. Manuf. Sci. Eng. **134**, 051015 (2012).

[54] A. Otto, S. Rauh, S. Ihlenfeldt, and G. Radons, Int. J. Adv. Manuf. Technol. **89**, 2613 (2017).

[55] J. Sieber, K. Engelborghs, T. Luzyanina, G. Samaey, and D. Roose, (2014), arXiv:1406.7144 [math.DS].

[56] L. F. Shampine, Appl. Num. Math. **52**, 113 (2005).

[57] W. Michiels and S.-I. Niculescu, *Stability and Stabilization of Time-Delay Systems* (SIAM, 2007).

[58] D. Bachrathy and G. Stépán, Period. Polytech., Mech. Eng. **56**, 81 (2012).

[59] G. W. Hill, Acta Math. **8**, 1 (1886).

[60] B. P. Lampe, E. N. Rosenwasser, and L. Berg, in *16th Int. Conf. MMAR, Miedzyzdroje, Poland* (2011) pp. 100–106.

[61] Y. Altintas, G. Stépán, D. Merdol, and Z. Dombovári, CIRP J. Manuf. Sci. Technol. **1**, 35 (2008).

[62] Y. Altintas, *Manufacturing Automation: Metal Cutting Mechanics, Machine Tool Vibrations, and CNC Design* (Cambridge University Press, 2012).

[63] T. Insperger and G. Stépán, R. Soc. Lond. Proc. Ser. A Math. Phys. Eng. Sci. **458**, 1989 (2002).

[64] M. Farkas, *Periodic Motions* (Springer, 1994).

## Appendix A: Stability analysis in the frequency domain

A frequency domain approach is suitable for the stability analysis of the modal dynamics Eq. (23) and Eq. (25) because exponential functions $e^{st}$ are eigenfunctions of the lag operator (cf. Eq. (13)). Here we present the methods for Eq. (23) but the results may be easily extended for Eq. (25).

For synchronized equilibria $\boldsymbol{x}_s(t) \equiv \boldsymbol{x}_s^*$, Eq. (23) with time invariant coefficient matrices $\mathbf{L}(t) = \mathbf{L}_0$ and $\mathbf{R}(t) = \mathbf{R}_0$ describes of the modal dynamics. Then, the exponential ansatz

$$\boldsymbol{q}_k(t) = \hat{\boldsymbol{q}}_{k,0}\, e^{st} \qquad (A1)$$

with $s \in \mathbb{C}$ (see [43, 47, 48, 57]) leads to the modal characteristic equation

$$\det\left[\mathbf{I}_n s - \mathbf{L}_0 - \mathbf{R}_0 \Lambda_k(s)\right] = 0, \qquad (A2)$$

where $\Lambda_k(s)$ os the eigenvalue of the operator $\mathcal{D}_k$, i.e.,

$$\mathcal{D}_k\, e^{st} = \Lambda_k(s)\, e^{st}. \qquad (A3)$$

Recall that $e^{-s\tau}$ is the eigenvalue of the lag operator $\mathcal{S}(\tau)$; see Eq. (13). When $\mathcal{D}_k$ can be written in the form Eq. (22), we have

$$\Lambda_k(s) = \sum_{r=1}^{R} \sigma_{r,k}\, e^{-s\tau_r}. \qquad (A4)$$

The the characteristic roots $s$ for network mode $k$, can be found by solving the characteristic equation Eq. (A2). If all characteristic roots are located in the left-half of the complex plane then the mode is stable. Although there are infinitely many characteristic roots, those with the largest real part, often called dominant roots, determine the stability. In this paper we compute these roots by using a multi-dimensional bisection method [37, 58]. As the parameters (e.g., the delays) are varied, roots can move into the right half complex plane resulting in an instability. The stability boundaries indicate the parameter values where roots cross the imaginary axis. By substituting $s = i\omega$, $\omega \geq 0$ into Eq. (A2) one may find these boundaries.

For synchronized periodic solutions $\boldsymbol{x}_s(t) = \boldsymbol{x}_s(t + T)$, where $T$ denotes the period, we use Hill's infinite determinant method to determine stability [59, 60]. The method is often used in engineering applications and it is also known as multifrequency approach [36, 37, 61–63]. For synchronized periodic solutions the coefficient matrices are periodic, that is, $\mathbf{L}(t) = \mathbf{L}(t+T)$ and $\mathbf{R}(t) = \mathbf{R}(t+T)$. From Floquet theory it is known that the solutions of Eq. (23) can be written as

$$\boldsymbol{q}_k(t) = \boldsymbol{p}_k(t)\, e^{st}, \quad \boldsymbol{p}_k(t) = \boldsymbol{p}_k(t + T), \qquad (A5)$$

where the complex numbers $s \in \mathbb{C}$ are called Floquet exponents; see [64]. The periodic part $\boldsymbol{p}_k(t)$ can be expanded using Fourier series

$$\boldsymbol{p}_k(t) = \sum_{l=-\infty}^{\infty} \hat{\boldsymbol{q}}_{k,l}\, e^{il\Omega t} \;\Rightarrow\; \boldsymbol{q}_k(t) = \sum_{l=-\infty}^{\infty} \hat{\boldsymbol{q}}_{k,l}\, e^{(s+il\Omega)t}, \qquad (A6)$$

where $\Omega = 2\pi/T$ is the frequency and $\hat{\boldsymbol{q}}_{k,l}$ are the Fourier coefficients. Similarly, the periodic matrices $\mathbf{L}(t)$ and $\mathbf{R}(t)$ can be expanded into Fourier series

$$\mathbf{L}(t) = \sum_{m=-\infty}^{\infty} \mathbf{L}_m\, e^{im\Omega t}, \quad \mathbf{R}(t) = \sum_{m=-\infty}^{\infty} \mathbf{R}_m\, e^{im\Omega t}. \qquad (A7)$$

Note that the Fourier coefficients $\mathbf{L}_m$ and $\mathbf{R}_m$ depend on the form of the synchronized periodic solution of the network, which is often available only numerically.

Putting Eq. (A6) and Eq. (A7) into the modal dynamics Eq. (23) yields

$$\sum_{m=-\infty}^{\infty} e^{im\Omega t} \sum_{l=-\infty}^{\infty} \mathbf{M}_{m,l}\, \hat{\boldsymbol{q}}_{k,l} = 0, \qquad (A8)$$

where the matrices $\mathbf{M}_{m,l}$ are given by

$$\mathbf{M}_{m,l} = \mathbf{I}_n(s+il\Omega)\,\delta_{m,l} - \mathbf{L}_{m-l} - \mathbf{R}_{m-l}\,\Lambda_k(s+il\Omega), \quad (A9)$$

and $\Lambda_k(s)$ are defined in Eq. (A3). Since in Eq. (A8) the coefficients for each harmonic $m$ must vanish, we obtain

$$\det \begin{bmatrix} \ddots & & \vdots & & \iddots \\ & \mathbf{M}_{-1,-1} & \mathbf{M}_{-1,0} & \mathbf{M}_{-1,1} & \\ \cdots & \mathbf{M}_{0,-1} & \mathbf{M}_{0,0} & \mathbf{M}_{0,1} & \cdots \\ & \mathbf{M}_{1,-1} & \mathbf{M}_{1,0} & \mathbf{M}_{1,1} & \\ \iddots & & \vdots & & \ddots \end{bmatrix} = 0. \qquad (A10)$$

This infinite determinant can be interpreted as the characteristic equation of the DDE Eq. (23) for periodic coefficient matrices. Note that the matrices $\mathbf{M}_{m,l}$ also depend on the modal index $k$. Notice that if the coefficient matrices $\mathbf{L}(t), \mathbf{R}(t)$ are constant, the higher harmonics in Eq. (A7) vanish, i.e., $\mathbf{L}_m = \mathbf{R}_m = \mathbf{0}$ for $m \neq 0$, and Eq. (A10) simplifies to Eq. (A2).

Again, stability is guaranteed when all Floquet exponents $s$ are located in the left-half of the complex plane. We use the multi-dimensional bisection method to compute the exponents and detect the stability boundaries in parameter space [37, 58] but one may find alternative methods in [51]. For a practical calculation of the determinant Eq. (A10), the infinite matrix $\mathbf{M}$ is truncated to a finite dimensional matrix by taking into account only a finite number of higher harmonics [36, 37, 61, 62]. Finally, we remark that ansatzes similar to Eq. (A1) or Eq. (A5) can also be made in the original system Eq. (8) leading to a complete frequency domain description of the network dynamics.

## Appendix B: Network modes for the examples

For simplicity we introduce the notation $\mathcal{S}(\tau_1) = \mathcal{S}_1$, $\mathcal{S}(\tau_2) = \mathcal{S}_2$. The operator-valued right and left eigenvectors for the all-to-all coupling Eq. (28) corresponding to the operator-valued eigenvalues Eq. (29) are given by

$$
\mathcal{V}_1 = \begin{bmatrix} 1 \\ 1 \\ 1 \\ 1 \\ 1 \end{bmatrix}, \quad
\mathcal{V}_2 = \begin{bmatrix} 1 \\ -\frac{3}{2} \\ -\frac{3}{2} \\ 1 \\ 1 \end{bmatrix}, \quad
\mathcal{V}_3 = \frac{1}{4\mathcal{S}_1 + \mathcal{S}_2} \begin{bmatrix} \mathcal{S}_1 \\ \mathcal{S}_1 \\ \mathcal{S}_1 \\ -(3\mathcal{S}_1 + \mathcal{S}_2) \\ \mathcal{S}_1 \end{bmatrix}, \quad
\mathcal{V}_4 = \begin{bmatrix} 0 \\ \frac{1}{2} \\ -\frac{1}{2} \\ 0 \\ 0 \end{bmatrix}, \quad
\mathcal{V}_5 = \frac{1}{3\mathcal{S}_1 + 2\mathcal{S}_2} \begin{bmatrix} \mathcal{S}_1 + \mathcal{S}_2 \\ -\frac{1}{2}\mathcal{S}_1 \\ -\frac{1}{2}\mathcal{S}_1 \\ \mathcal{S}_1 + \mathcal{S}_2 \\ -(2\mathcal{S}_1 + \mathcal{S}_2) \end{bmatrix},
$$
(B1)

and

$$
\begin{aligned}
\mathcal{U}_1 &= \begin{bmatrix} \frac{1}{5} \frac{13\mathcal{S}_1^2 + 9\mathcal{S}_1\mathcal{S}_2 + 3\mathcal{S}_2^2}{(4\mathcal{S}_1 + \mathcal{S}_2)(3\mathcal{S}_1 + 2\mathcal{S}_2)} & \frac{1}{5} & \frac{1}{5} & \frac{\mathcal{S}_1}{4\mathcal{S}_1 + \mathcal{S}_2} & \frac{1}{5} \frac{2\mathcal{S}_1 + 3\mathcal{S}_2}{3\mathcal{S}_1 + 2\mathcal{S}_2} \end{bmatrix}, \\
\mathcal{U}_2 &= \begin{bmatrix} \frac{1}{5} & -\frac{1}{5} & -\frac{1}{5} & 0 & \frac{1}{5} \end{bmatrix}, \\
\mathcal{U}_3 &= \begin{bmatrix} 1 & 0 & 0 & -1 & 0 \end{bmatrix}, \\
\mathcal{U}_4 &= \begin{bmatrix} 0 & 1 & -1 & 0 & 0 \end{bmatrix}, \\
\mathcal{U}_5 &= \begin{bmatrix} 1 & 0 & 0 & 0 & -1 \end{bmatrix}.
\end{aligned}
$$
(B2)

The operator-valued right and left eigenvectors for general coupling Eq. (32) corresponding to $\mathcal{D}_1$, $\mathcal{D}_2$ and $\mathcal{D}_3$ in Eq. (33) and $\mathcal{D}_{4,5}$ in Eq. (34) are given by

$$
\mathcal{V}_1 = \begin{bmatrix} 1 \\ 1 \\ 1 \\ 1 \\ 1 \end{bmatrix}, \quad
\mathcal{V}_2 = \begin{bmatrix} 1 \\ -2 \\ -2 \\ 1 \\ 1 \end{bmatrix}, \quad
\mathcal{V}_3 = \frac{1}{2} \frac{1}{(\mathcal{S}_1 + \mathcal{S}_2)(\mathcal{S}_1 - 2\mathcal{S}_2)} \begin{bmatrix} \mathcal{S}_1^2 - 2\mathcal{S}_2^2 \\ -\mathcal{S}_1^2 \\ -\mathcal{S}_1^2 \\ \mathcal{S}_1^2 - 2\mathcal{S}_2^2 \\ -(\mathcal{S}_1^2 - 2\mathcal{S}_1\mathcal{S}_2 - 2\mathcal{S}_2^2) \end{bmatrix},
$$

$$
\mathcal{V}_{4,5} = \frac{1}{(\mathcal{S}_1^2 - \mathcal{S}_1\mathcal{S}_2 + 2\mathcal{S}_2^2)(7\mathcal{S}_1^2 + 8\mathcal{S}_1\mathcal{S}_2 + 2\mathcal{S}_2^2)}
$$

$$
\times \begin{bmatrix}
\mathcal{S}_1(\mathcal{S}_1^3 - \mathcal{S}_1\mathcal{S}_2^2 - \mathcal{S}_2^3) & \mathcal{S}_1(2\mathcal{S}_1^3 + 2\mathcal{S}_1^2\mathcal{S}_2 + 5\mathcal{S}_1\mathcal{S}_2^2 + 4\mathcal{S}_2^3) \\
\mathcal{S}_1^4 + 6\mathcal{S}_1^2\mathcal{S}_2^2 + 7\mathcal{S}_1\mathcal{S}_2^3 + 2\mathcal{S}_2^4 & \mathcal{S}_1(2\mathcal{S}_1^3 - 5\mathcal{S}_1^2\mathcal{S}_2 - 3\mathcal{S}_1\mathcal{S}_2^2 + 2\mathcal{S}_2^3) \\
-6\mathcal{S}_1^4 - \mathcal{S}_1^3\mathcal{S}_2 - 2\mathcal{S}_1^2\mathcal{S}_2^2 - 7\mathcal{S}_1\mathcal{S}_2^3 - 2\mathcal{S}_2^4 & \mathcal{S}_1(2\mathcal{S}_1^3 - 5\mathcal{S}_1^2\mathcal{S}_2 - 3\mathcal{S}_1\mathcal{S}_2^2 + 2\mathcal{S}_2^3) \\
\mathcal{S}_1(\mathcal{S}_1^3 - \mathcal{S}_1\mathcal{S}_2^2 - \mathcal{S}_2^3) & -5\mathcal{S}_1^4 + \mathcal{S}_1^3\mathcal{S}_2 - 3\mathcal{S}_1^2\mathcal{S}_2^2 - 10\mathcal{S}_1\mathcal{S}_2^3 - 4\mathcal{S}_2^4 \\
\mathcal{S}_1(\mathcal{S}_1^3 - \mathcal{S}_1\mathcal{S}_2^2 - \mathcal{S}_2^3) & \mathcal{S}_1(2\mathcal{S}_1^3 + 2\mathcal{S}_1^2\mathcal{S}_2 + 5\mathcal{S}_1\mathcal{S}_2^2 + 4\mathcal{S}_2^3)
\end{bmatrix},
$$
(B3)

and

$$
\begin{aligned}
\mathcal{U}_1 &= \begin{bmatrix} \frac{1}{6} \frac{9\mathcal{S}_1^3 + 16\mathcal{S}_1^2\mathcal{S}_2 + 12\mathcal{S}_1\mathcal{S}_2^2 + 4\mathcal{S}_2^3}{(\mathcal{S}_1 + \mathcal{S}_2)(7\mathcal{S}_1^2 + 8\mathcal{S}_1\mathcal{S}_2 + 2\mathcal{S}_2^2)} & \frac{(\mathcal{S}_1 + \mathcal{S}_2)(4\mathcal{S}_1 + \mathcal{S}_2)}{21\mathcal{S}_1^2 + 24\mathcal{S}_1\mathcal{S}_2 + 6\mathcal{S}_2^2} & \frac{3\mathcal{S}_1^2 + 3\mathcal{S}_1\mathcal{S}_2 + \mathcal{S}_2^2}{21\mathcal{S}_1^2 + 24\mathcal{S}_1\mathcal{S}_2 + 6\mathcal{S}_2^2} & \frac{\mathcal{S}_1(6\mathcal{S}_1 + 5\mathcal{S}_2)}{21\mathcal{S}_1^2 + 24\mathcal{S}_1\mathcal{S}_2 + 6\mathcal{S}_2^2} & \frac{1}{6} \frac{\mathcal{S}_1 + 2\mathcal{S}_2}{\mathcal{S}_1 + \mathcal{S}_2} \end{bmatrix}, \\
\mathcal{U}_2 &= \begin{bmatrix} -\frac{1}{3} \frac{\mathcal{S}_2(2\mathcal{S}_1^2 - 3\mathcal{S}_1\mathcal{S}_2 + 2\mathcal{S}_2^2)}{(\mathcal{S}_1 - 2\mathcal{S}_2)(\mathcal{S}_1^2 - \mathcal{S}_1\mathcal{S}_2 + 2\mathcal{S}_2^2)} & -\frac{1}{3} \frac{\mathcal{S}_1^2 - \mathcal{S}_1\mathcal{S}_2 + \mathcal{S}_2^2}{\mathcal{S}_1^2 - \mathcal{S}_1\mathcal{S}_2 + 2\mathcal{S}_2^2} & -\frac{1}{3} \frac{\mathcal{S}_2^2}{\mathcal{S}_1^2 - \mathcal{S}_1\mathcal{S}_2 + 2\mathcal{S}_2^2} & \frac{1}{3} \frac{\mathcal{S}_1\mathcal{S}_2}{\mathcal{S}_1^2 - \mathcal{S}_1\mathcal{S}_2 + 2\mathcal{S}_2^2} & \frac{1}{3} \frac{\mathcal{S}_1 - \mathcal{S}_2}{\mathcal{S}_1 - 2\mathcal{S}_2} \end{bmatrix}, \\
\mathcal{U}_3 &= \begin{bmatrix} 1 & 0 & 0 & 0 & -1 \end{bmatrix}, \\
\mathcal{U}_{4,5} &= \begin{bmatrix} 0 & 1 & -1 & 0 & 0 \\ 1 & 0 & 0 & -1 & 0 \end{bmatrix}.
\end{aligned}
$$
(B4)

## Appendix C: Details of the Hodgkin-Huxley model

The nonlinear functions used in the the Hodgkin-Huxley model Eq. (35) are

$$
\alpha_m(V) = \frac{0.1\,(V + 40)}{1 - e^{-\frac{V+40}{10}}}, \qquad \beta_m(V) = 4\,e^{-\frac{V+65}{18}},
$$

$$
\alpha_h(V) = 0.07\,e^{-\frac{V+65}{20}}, \qquad \beta_h(V) = \frac{1}{1 + e^{-\frac{V+35}{10}}}, \quad \text{(C1)}
$$

$$
\alpha_n(V) = \frac{0.01\,(V + 55)}{1 - e^{-\frac{V+55}{10}}}, \qquad \beta_n(V) = 0.125\,e^{-\frac{V+65}{80}}.
$$

while the parameters used in Eq. (35) are given in Table I.

TABLE I. Parameters for Hodgkin-Huxley neurons.

| | | |
|---|---|---|
| $V_{\mathrm{Na}} = 50$ mV | $g_{\mathrm{Na}} = 120\frac{\mathrm{mS}}{\mathrm{cm}^2}$ | $C = 1\frac{\mu\mathrm{F}}{\mathrm{cm}^2}$ |
| $V_{\mathrm{K}} = -77$ mV | $g_{\mathrm{K}} = 36\frac{\mathrm{mS}}{\mathrm{cm}^2}$ | $I = 20\frac{\mu\mathrm{A}}{\mathrm{cm}^2}$ |
| $V_{\mathrm{L}} = -54.4$ mV | $g_{\mathrm{L}} = 0.3\frac{\mathrm{mS}}{\mathrm{cm}^2}$ | |